Structure and Evolution of Winter Cyclones in the Central United States and Their Effects on the Distribution of Precipitation. Part II: Arctic Fronts

PENG-YUN WANG,* JONATHAN E. MARTIN, JOHN D. LOCATELLI, AND PETER V. HOBBS

Atmospheric Sciences Department, University of Washington, Seattle, Washington

(Manuscript received 3 May 1994, in final form 3 October 1994)

ABSTRACT

The structure and evolution of a shallow but intense cold front (commonly referred to as an *arctic front*) and its associated precipitation features that passed through the central United States from 0000 UTC 9 March to 0000 UTC 10 March 1992 are studied with the aid of observations and outputs from a numerical simulation using the Pennsylvania State University–National Center for Atmospheric Research Mesoscale Model MM4.

Located above the arctic front was a region of midtropospheric, frontogenetical confluence that was attended by a thermally direct vertical circulation. A large banded precipitation feature, for the most part located behind the arctic front, was produced by ice crystals from upper-level clouds (formed by the frontogenetical confluence) falling into low-level stratocumulus associated with the arctic front. The arctic front at the surface separated a region where the precipitation reaching the ground was solid from an adjacent region where the precipitation was liquid. A westward-moving, low-level jet behind the arctic front produced upslope flow over the high terrain of the northern Great Plains, which contributed to heavy snowfalls in this region.

A portion of the arctic front that moved southward, west of a low pressure center, was characterized by sharp drops in temperature and dewpoint and an increase in wind speed. However, the arctic front was not associated with either a pressure trough or much change in wind direction. The proximity of arctic fronts to such nonfrontal features as lee troughs and/or drylines often leads to the latter being misanalyzed as cold fronts.

1. Introduction

During winter, the central United States is often affected by the rapid southward migration of continental polar air masses that have cooled, sometimes for many days, over snow-covered regions in central and Arctic Canada (e.g., Wexler 1936). The temperature lapse rate in the overlying air is often isothermal up to about 3–4 km (e.g., Showalter 1939). As arctic air travels southward into the central United States, it becomes less stable due to the transfer of heat from the ground. The boundary between the cold arctic air and the warmer air to the south is often very sharp. The warm edge of this knifelike transition zone is called the *arctic front* (or "northerly surge" or "cold surge" when it is located along the east edge of Rockies or "blue norther" in Texas). As arctic fronts move into the High Plains of the United States, they can produce heavy precipitation in regions of rising topography and frontogenesis along the front. The arctic front often marks a transition zone between snow or freezing rain to the north and rain to the south.

When cyclogenesis occurs in the central United States, due to the migration of a synoptic-scale shortwave over the Rocky Mountains, the high topography to the west virtually ensures that a southward-moving arctic front will move along the eastern slopes of the Rocky Mountains west of the developing low pressure center and northwest of the surface pressure trough that formed in the lee of the Rockies; we refer to the latter feature as a *drytrough* (Martin et al. 1995).

One of the earliest applications of the Norwegian polar front model to weather systems in the United States can be used to illustrate some of the important features of arctic fronts. Shown in Fig. 1 is an analysis from Rossby and Weightman (1926). They identified the front labeled C_p as a continental polar front, although it is actually a drytrough (Martin et al. 1995). In Fig. 1, the arctic front is labeled C_2 west of the surface low and C_1 to the east. Rossby and Weightman noted that C_2 had no wind shift across it but was easily located by a temperature change. The absence of a wind shift at the nose of the front is a consequence of the lack of a pressure trough. There is, however, an increase in the wind speed across C_2 since the arctic front is located near the maximum spreading of the isobars, a region of strong surface diffluence.

Bluestein (1993) noted that the southward movement of cold anticyclones in the lee of the Rocky Mountains is occasionally accompanied by a rapid increase in wind speed and gustiness, but no wind shift.

* Permanent affiliation: Chinese Academy of Meteorological Sciences, Beijing, People's Republic of China.

Corresponding author address: Dr. Peter V. Hobbs, Department of Atmospheric Sciences, AK-40, University of Washington, Seattle, WA 98195.

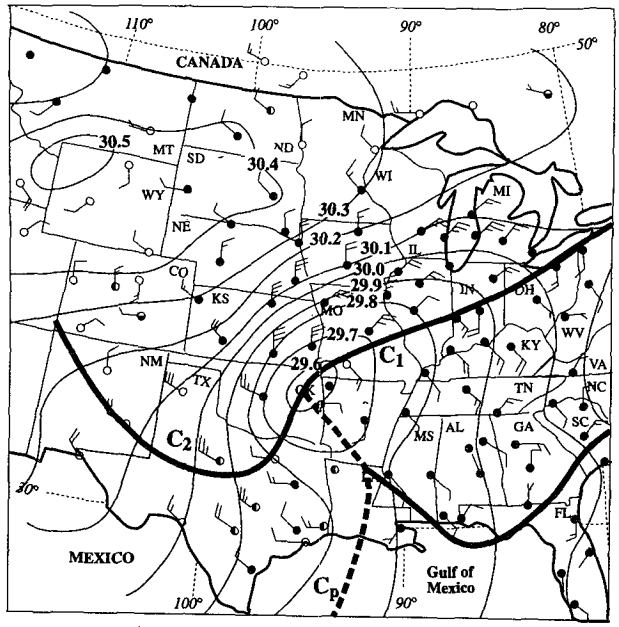

FIG. 1. Rossby and Weightman's (1926) surface analysis for 0800 UTC 18 February 1926. Solid lines are isobars (in inches). For each surface station sky cover, wind direction, and speed are shown. Sky cover is shown using the following symbols: open circle, clear; half-circle shaded, scattered cloud; fully shaded circle, overcast. Wind speeds are indicated by short bar, 2.5 m s^{-1}; long bar, 5 m s^{-1}. See text for explanations for the heavy lines labeled C_1, C_2, and C_p.

The fact that the arctic front is located behind the drytrough and is not associated with a pressure trough can lead to misanalysis. Thus, the drytrough is often misanalyzed as a cold front. Several examples of this type of misanalysis are given by Hobbs et al. (1990). As cyclones in the central United States develop and move eastward, the arctic front approaches the drytrough and can eventually occupy its northern portion. The extension of the arctic air to the east of the center of the cyclone often results in the formation of an intense surface front that has the characteristics of a stationary or warm front. This feature is labeled C_1 in Fig. 1.

In this paper we describe an arctic front that moved through the central United States from 8 to 10 March 1992. This front was well documented by the intensive observing facilities of the STORM-Fronts Experiment System Test (STORM-FEST), which included high temporal and spatial resolution rawinsondes, profilers, aircraft, surface observations, and conventional and Doppler radars. We will describe the structure, development, and evolution of this arctic front and its associated precipitation features during the period 0000 UTC 9 March to 0000 UTC 10 March 1992. In addition to utilizing the extensive observations provided by STORM-FEST, we have utilized the Pennsylvania State University–National Center for Atmospheric Research (NCAR) Mesoscale Model (MM4, version 8) to diagnose the front.

2. Comparison of numerical model simulations and observations

The MM4 model has been described by Anthes and Warner (1978) and Anthes et al. (1987). The version of this model we used includes a high-resolution planetary boundary layer (Blackadar 1979; Zhang and Anthes 1982) and prognostic equations for water vapor, cloud water, and rainwater. The terrain is represented by actual heights on a 0.5° × 0.5° latitude–longitude grid. The domain contains 61 × 61 grid points with a grid size of 45 km centered at 40° N, 96°W. The model atmosphere is divided into 23 layers from the surface to 50 mb; a sigma vertical coordinate system is used.

The model was initialized using the National Meteorological Center (NMC) gridded data as a "first-guess" field, supplemented by NMC and global operational surface and rawinsonde data, and snow cover and land-use data prepared and maintained by NCAR. The lateral boundary conditions were linearly interpolated in time by using observational data at 12-h intervals. The model simulations were started at 0000 UTC 9 March and ended at 0000 UTC 10 March 1992.

Described below are comparisons between the model simulated and the observed geopotential height and temperature fields at upper levels, surface pressure and temperature, and precipitation. Since the simulations were initiated at 0000 UTC 9 March, we begin our comparisons with the 12-h forecast data and observations at 1200 UTC 9 March.

a. 500-mb geopotential height and temperature fields

At 1200 UTC 9 March 1992, the axis of the analyzed 500-mb trough extended from North Dakota to Arizona, with the lowest geopotential height located in eastern Colorado. A distinct trough was located in south-central Canada. The southern trough was characterized by a significant baroclinic zone on its eastern edge, with the coldest air (−25°C) centered over Denver, Colorado. Accompanying the strong thermal gradient east of the trough axis was a jet streak that ran through western Texas into extreme south western Missouri (Fig. 2a). By 0000 UTC 10 March, the northern trough had moved eastward and was located along the border between the Dakotas and Minnesota, with the southern trough extending from the panhandle of Oklahoma through western Texas (Fig. 2b). The baroclinic zone had tightened and moved eastward so that by this time it was located in eastern Texas and stretched northward into central Missouri. The MM4 12-h model run valid for 1200 UTC 9 March (Fig. 2c) is very similar to the analysis (Fig. 2a): it shows the same trough location, with a minimum in geopotential height (of 5455 m) and a minimum temperature (of −25.5°C) at the Colorado–Kansas border. The model-simulated wind field (not shown) is also in good agreement with the observations. The 24-h model simulation

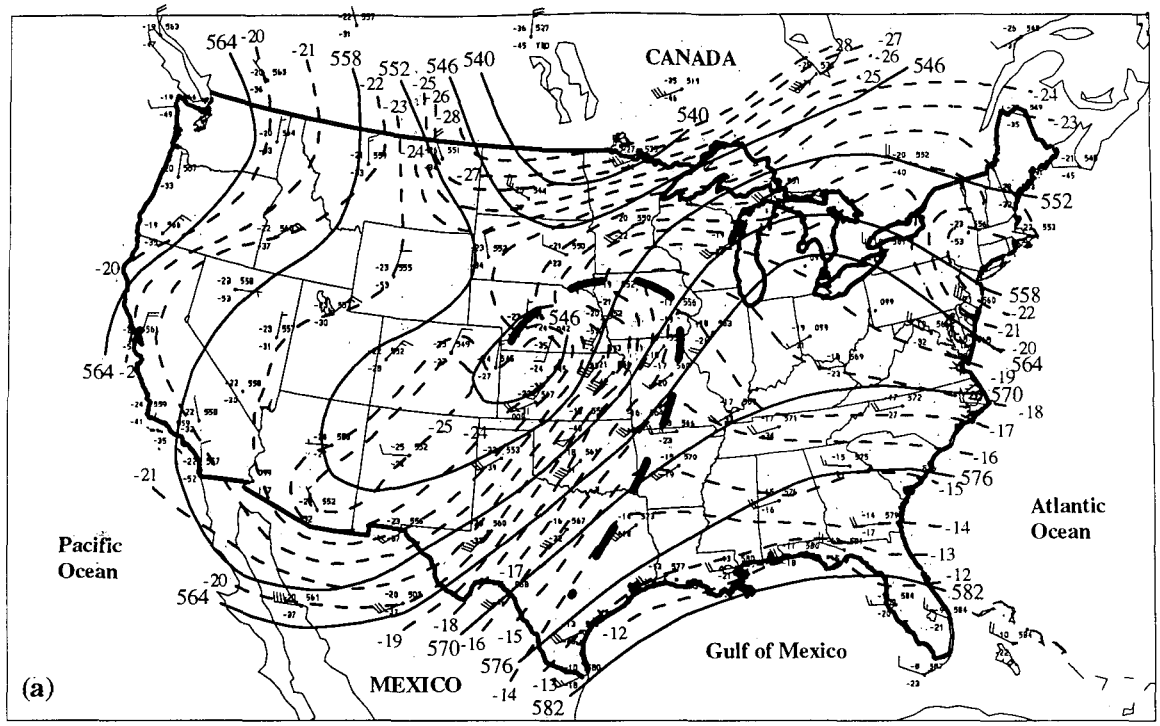

FIG. 2. (a) The 500-mb analysis for 1200 UTC 9 March 1992. Shown are geopotential heights (continuous lines, labeled in tens of meters and contoured every 60 m) and isotherms (dashed lines, labeled in degrees Celsius and contoured every 2°C). Heavy dashed line shows the boundary of cold-air advection at 500 mb. (b) As for (a) but for 0000 UTC 10 March 1992. (c) MM4 model simulations of 500-mb geopotential heights (continuous lines, labeled in meters and contoured every 60 m) and temperatures (dashed lines, labeled in degrees Celsius and contoured every 2°C) at 1200 UTC 9 March 1992. (d) As for (c) but for 0000 UTC 10 March 1992.

valid for 0000 UTC 10 March (Fig. 2d) is also similar to the analysis (Fig. 2b).

b. 850-mb geopotential height and temperature fields

At 1200 UTC 9 March, an 850-mb trough extended from southern Lake Superior to the panhandle of Oklahoma. Embedded within this trough was the upper portion of the shallow arctic frontal zone, which stretched from near the Great Lakes to southeast Colorado (Fig. 3a). By 0000 UTC 10 March, the trough and frontal zone had moved eastward into central Missouri and eastern Oklahoma (Fig. 3b). This movement was accompanied by a significant increase in the magnitude of the temperature gradient at 850 mb. Again, the MM4 model simulated the geopotential height and temperature fields quite well (Fig. 3c and 3d).

c. Sea level pressure and temperature fields

At 1200 UTC 9 March, the low pressure center was located in western Kansas, having moved there from extreme eastern Colorado in the previous 12 h. The arctic front stretched southwestward from Lake Mich-

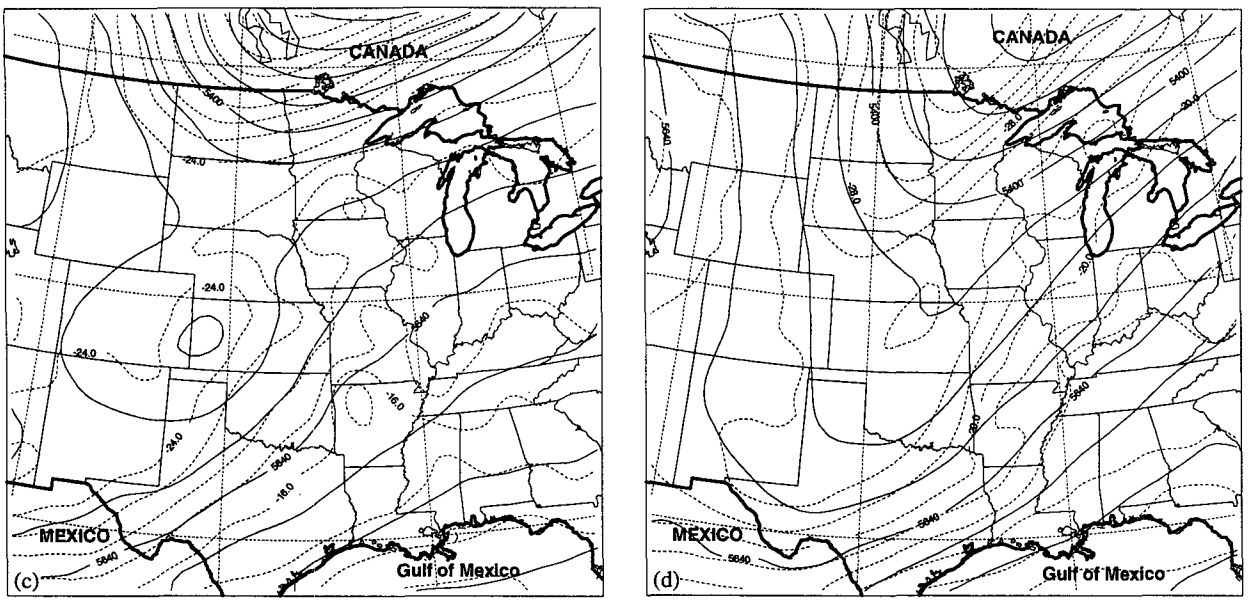

FIG. 2. (*Continued*)

igan, through the low pressure center, and into the northern Texas panhandle (Fig. 4a). Ahead of the front, in central Oklahoma and eastern Texas, was a drytrough, which was aligned north–south (Fig. 4a). The evolution of this drytrough has been described by Martin et al. (1994). By 0000 UTC 10 March, the arctic front had moved southeastward into central Missouri. The drytrough preceded the arctic front through western Arkansas and northwestern Louisiana (Fig. 4b). The MM4 model-simulated sea level pressure and temperature fields have essentially the same locations for the low pressure center and the arctic front as the analysis (Figs. 4c and 4d). The model simulations also reproduced quite well the arctic front, the frontal trough, and the advance of the arctic front toward the drytrough (not shown).

Figures 4a and 4b show no noticeable pressure trough at the surface location of the arctic front west of the low pressure center. Also, there is not a strong wind shift at this location, although there is a general increase in wind speed behind the front and a sudden drop in temperature and dewpoint. The lack of a trough and wind shift at the arctic front, coupled with its proximity to the isobaric minimum associated with the drytrough, often results in the drytrough being misanalyzed as a surface cold front. Indeed, that is what happened in this case since the NWS marked the drytrough as a cold front. To help avoid this mistake, we recommend that arctic fronts be marked and tracked separately from deeper cold fronts. Notice that the portion of the arctic front that extended to the east of the low pressure center at the surface was associated with an obvious pressure trough. We will see in section 3 that the arctic front in that location acted as a stationary front at its leading edge and that above it there was a strong zone of confluent frontogenesis.

d. Precipitation

Comparisons of the National Climatic Data Center (NCDC) accumulated rainfalls with the MM4 simulated accumulated rainfalls for the periods 1000–1300 UTC 9 March and 2300 UTC 9 March–0200 UTC 10 March 1992 are shown in Fig. 5. At 1000–1300 UTC 9 March the precipitation associated with the arctic front was located on a line stretching from west central Nebraska northeastward to Wisconsin (Fig. 5a). The precipitation moved gradually southeastward; between 2300 UTC 9 March and 0200 UTC 10 March it ran from east of Kansas City to Lake Huron (Fig. 5b). The aerial coverage of the precipitation associated with the arctic front was rather skillfully simulated by the MM4 model (Figs. 5c and 5d), although the model predicted higher amounts of precipitation for the first period and lower amounts for the second period than those measured. Not surprisingly, the model did not do quite as well in capturing the precipitation amounts associated with the squall lines farther south.

e. Vertical cross sections

Analyzed vertical cross sections, based on STORMFEST rawinsonde and research aircraft data, and the corresponding MM4 cross sections were generally in excellent agreement (not shown).

f. Summary

The comparisons discussed above show that the MM4 24-h model simulation was quite accurate with

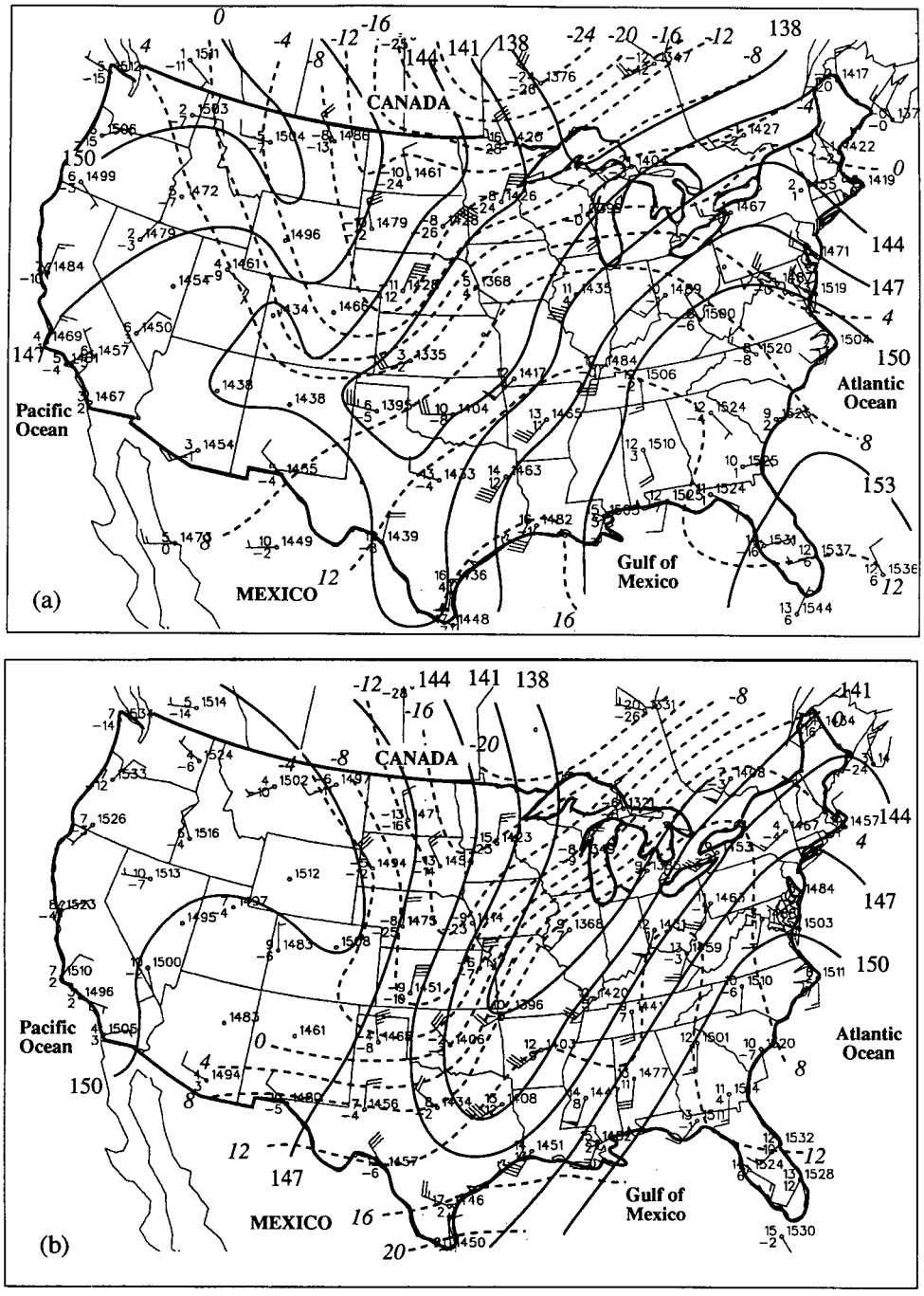

FIG. 3. (a) The 850-mb analysis for 1200 UTC 9 March 1992. The geopotential heights are shown by continuous lines, labeled in tens of meters and contoured every 30 m. The temperatures are shown by dashed lines, labeled in degrees Celsius and contoured every 4°C. (b) As for (a) but for 0000 UTC 10 March 1992. (c) MM4 model simulations of 850-mb geopotential heights (continuous lines, labeled in meters and contoured every 30 m) and temperatures (dashed lines, labeled in degrees Celsius and contoured every 2°C) at 1200 UTC 9 March 1992. (d) As for (c) but for 0000 UTC 10 March 1992.

respect to the arctic front. Moreover, the model simulation provides a high-resolution (45 km in space and 15 min in time) and dynamically consistent dataset. Therefore, we will use the model simulation in our subsequent analyses of the structure, development, and evolution of the arctic front and the various precipita-

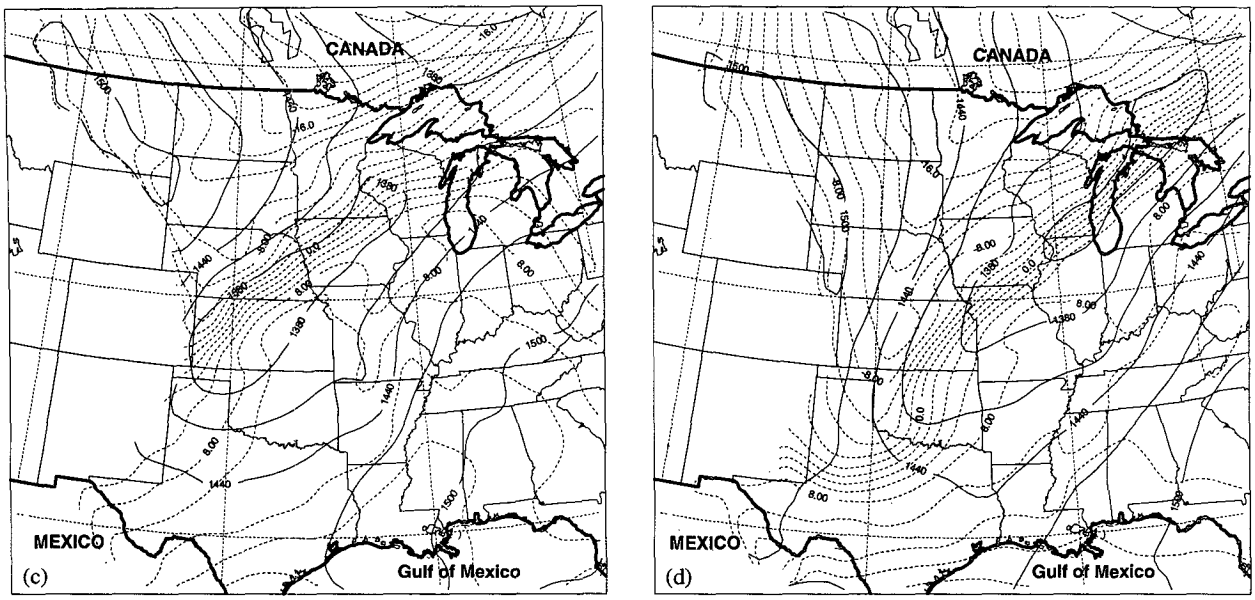

FIG. 3. (*Continued*)

tion bands associated with it. However, when model simulations differ significantly from the observations the later will be used.

3. Dynamics, thermodynamics, and microphysics of the arctic front

The MM4 gridpoint data can be used to study the 3D dynamical and thermodynamical structure of the arctic front and its evolution.

a. 1200 UTC 9 March 1992

Shown in Fig. 6 are the MM4 model simulations of the 700-mb geopotential height and temperature fields for 1200 UTC 9 March. There was another baroclinic zone to the northwest of Lake Superior at 700 mb but it was associated with a trough in western Ontario; this baroclinic zone was responsible for the deep, cold-air advection over northern Minnesota and the Dakotas at this time (see also Fig. 2c). Figure 6 shows a discontinuity in the overall temperature gradient at 700 mb that runs from near Minneapolis southwestward to north-central Nebraska (note the positions of the −8° and −10°C isotherms in Fig. 6). This discontinuity marks the boundary between the cold- and warm-air advection regions that overlie the low-level arctic air. The MM4 model cross sections from southern Lake Winnipeg to southern Illinois (through line *AB* in Fig. 6) are shown in Fig. 7. The potential temperature structure along this cross section (Fig. 7a) might suggest that the arctic front was an extremely deep feature since the 288-K isentrope (which marks the leading edge of the arctic air at the surface) exhibits a significant vertical slope up to 520 mb. The cross section of equivalent potential temperature shown in Fig. 7b gives a similar impression. However, the temperature cross section (Fig. 7c) shows that the arctic frontal inversion was at about 800 mb; this confirms the shallow nature of the arctic air. The isothermal lapse rate that is characteristic of arctic air was modified by surface heating and subsequent mixing as the arctic air pushed southward; this produced the well-mixed surface layer shown in Fig. 7c. Directly above this arctic air was a deep baroclinic zone (Fig. 6). Figure 7c shows that this baroclinic zone was characterized by warm-air advection at its front edge and cold-air advection everywhere else. The juxtaposition of cold- and warm-air advection was produced by an upper-level horizontally confluent flow superposed on a baroclinic zone in northwest Wisconsin (Fig. 6).

To assess the dynamical significance of this confluence, we used the MM4 model data to calculate horizontal frontogenesis F contributed by horizontal flow (deformation and convergence) using the expression (Ogura and Portis 1982)

$$F = \frac{d}{dt}|\nabla\theta| = \frac{|\nabla\theta|}{2}|\mathrm{def}_r|\cos 2\beta - \frac{|\nabla\theta|}{2}D, \quad (1)$$

where

$$\mathrm{def}_r = [(u_x - v_y)^2 + (v_x + u_y)^2]^{1/2},$$

and β is the angle from the axis of dilatation to the potential temperature θ lines. The subscripts x and y denote derivatives with respect to x and y, respectively. Here D is the horizontal divergence. The first term on the right side of (1) is due to horizontal deformation and the second term to convergence.

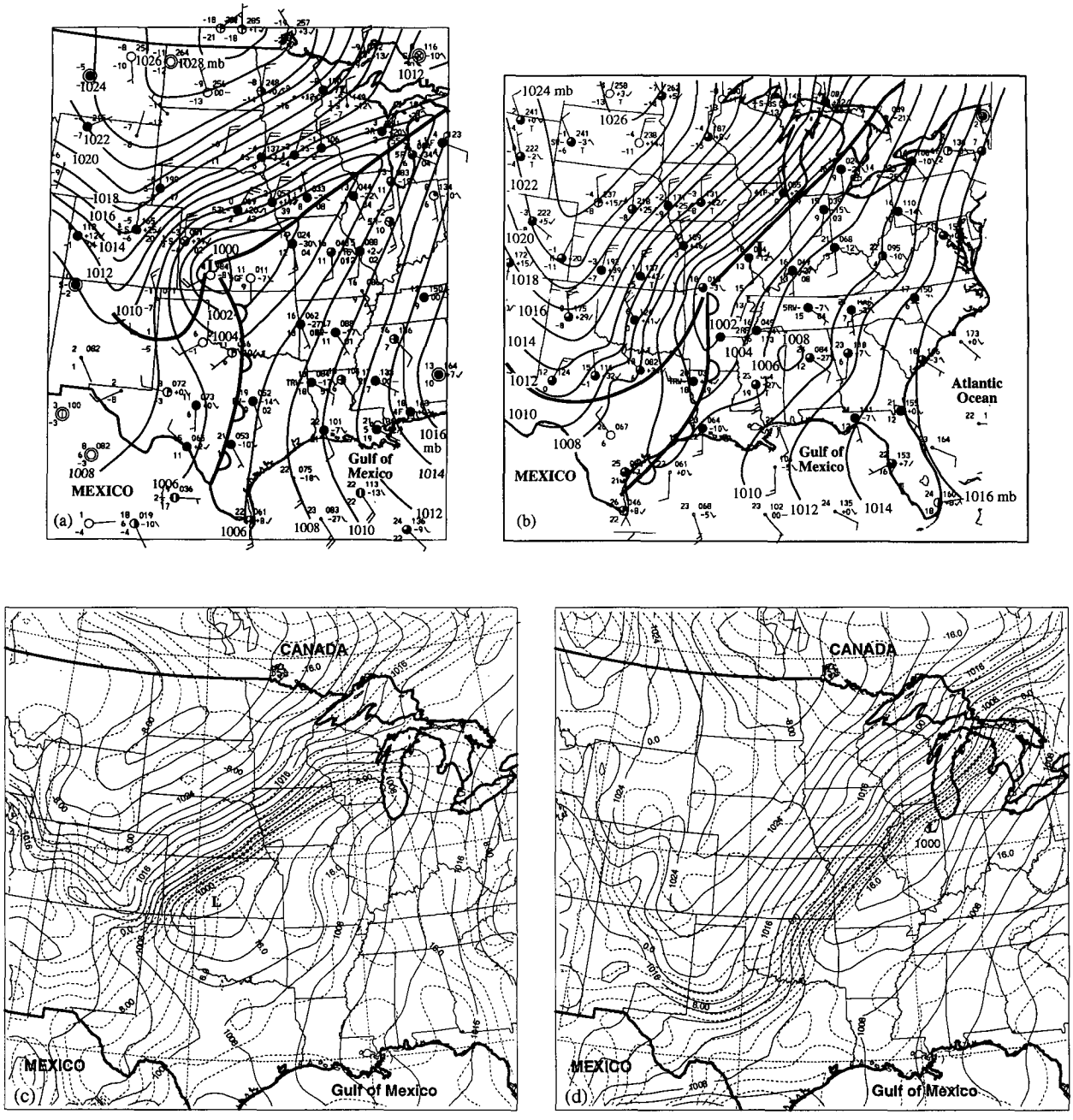

FIG. 4. (a) Sea level pressure analysis for 1200 UTC 9 March 1992. Solid lines are isobars (labeled in millibars and contoured every 2 mb). Here *L* marks the location of the low pressure center on the surface; the position of the arctic front at the surface is indicated by the heavy solid line and the drytrough is indicated by the scalloped line. For each surface station the following data is shown: temperature (°C, upper left of the station symbol), dewpoint temperature (°C, lower left of station symbol), sky cover (center of station symbol), wind direction and speed, and present weather. Sky cover is shown using the following symbols: open circle, clear; half-circle shaded, scattered cloud; unshaded vertical strip within otherwise shaded circle, broken cloud; fully shaded circle, overcast; and "X," sky obscured. Wind speeds are indicated by circle around a circle, calm; short bar, 2.5 m s^{-1}; long bar, 5 m s^{-1}; and flag, 25 m s^{-1}. Present weather symbols: R (rain), W (shower), L (drizzle), H (haze), S (snow), F (fog), ZR (freezing rain), BS (blowing snow), and K (smoke). A plus or minus sign after the precipitation type indicates heavy or light precipitation, respectively. (b) As for (a) but for 0000 UTC 10 March 1992. (c) MM4 model simulations of sea level pressures (continuous lines, labeled in millibars and contoured every 2 mb) and surface temperatures (dashed lines, labeled in degrees Celsius and contoured every 2°C) at 1200 UTC 9 March 1992. (d) As same for (c) but for 0000 UTC 10 March 1992.

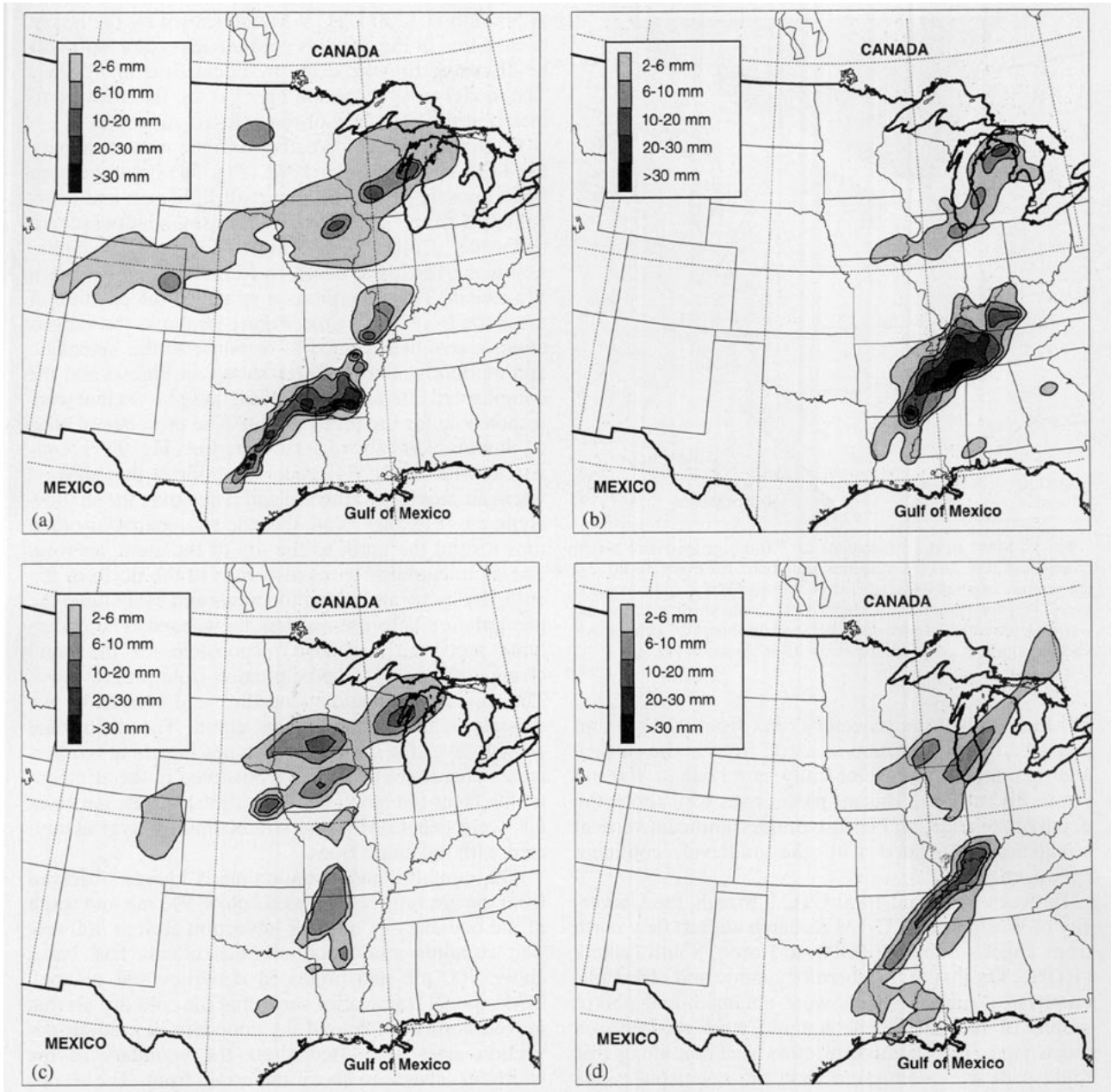

FIG. 5. (a) National Climatic Data Center accumulated precipitation for the period 1000–1300 UTC 9 March 1992. (b) As for (a) but for the period 2300 UTC 9 March–0200 UTC 10 March 1992. (c) As for (a) but from MM4 model simulations. (d) As for (b) but from MM4 model simulations.

Figure 7d shows frontogenesis values for a vertical cross section through *AB* in Fig. 6. The surface frontal position is characterized by a strong maximum in frontogenesis (80×10^{-10} K m^{-1} s^{-1}). The midlevel confluence just discussed also manifests itself as a maximum in frontogenesis (more than 30×10^{-10} K m^{-1} s^{-1}). Since this midlevel confluence was frontogenetical, it was accompanied by a thermally direct vertical circulation. We will hereafter refer to this midlevel frontogenesis region as the zone of confluent frontogenesis. The effect of the vertical circulation on the trajectory of air parcels is shown in Fig. 8.

Figure 8a shows the backward trajectory for an air parcel originating at point "PA" in Fig. 7c. This parcel sank and curved anticyclonically as it approached the arctic front from the north (from PA′ to PA) but it remained entirely within the arctic air mass. Figure 8b shows the computed trajectory of a parcel beginning on the warm-air advection side of the confluent frontogenetical region at 700 mb (from point "PB" in Fig.

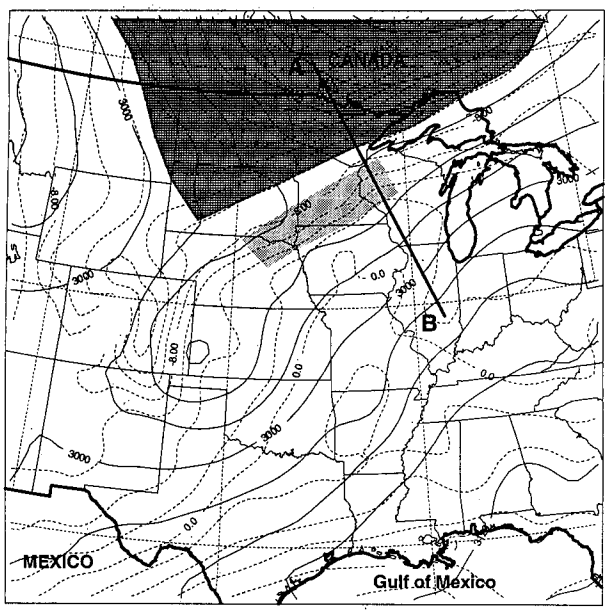

FIG. 6. MM4 model simulations of 700-mb geopotential height (continuous line, labeled in meters and contoured every 30 m) and temperature (dashed lines, labeled in degrees Celsius and contoured every 2°C) for 1200 UTC 9 March 1992. Light shading shows the warm-air advection region, and dark shading shows the cold-air advection region. A cross section along *AB* is shown in Fig. 7.

7c). Notice that the trajectory rises from 920 mb and just ahead of the position of arctic front at the surface and then moves anticyclonically as it rises to 700 mb (from PB′ to PB). This air parcel rises well above the depth of the arctic air because of the significant vertical circulation associated with the midlevel, confluent frontogenesis.

Between 1200 and 1400 UTC 9 March, the University of Washington's C-131 research aircraft flew north from Topeka, Kansas (TOP), to Huron, South Dakota (HON). On this flight, thermodynamic and cloud microphysical measurements were obtained, and photographs of the clouds encountered were recorded on video tape. Two composite cross sections along this flight path were composed from the rawinsonde data from Topeka; Omaha, Nebraska (OMA); Storm Lake, Iowa (SLB); and Huron; from aircraft data, and from surface observations along the path of the aircraft. Cloud-top information was obtained from satellite observations and from the airborne video.

Figure 9a shows the wind and thermodynamic structure, and Fig. 9b shows the flight-path and cloud and microphysical information. The positions of the arctic air, cold-air advection, and warm-air advection above the arctic air (confluent frontogenesis) revealed by these data are consistent with the MM4 model results for the cross section taken farther east (Fig. 7). However, note the intrusion of slightly cooler, lower-θ_e air overrunning the warm-air advection above the arctic front. This intrusion was part of the cold-air advection at 500 mb at 1200 UTC 9 March shown by the heavy dashed line in Fig. 2a; this cold-air advection aloft will be discussed in more detail by Locatelli et al. (1995). The model cross section in Fig. 7 is too far eastward to intercept the boundary of the cold-air advection.

From the National Weather Service radar summary for 1135 UTC 9 March 1992 (Fig. 5a) it can be seen that a loosely organized region of light rain and snow stretched from Green Bay, Wisconsin, southwestward to Denver, Colorado. The most widespread precipitation was over Iowa, southern Minnesota, and western Wisconsin. This precipitation straddled the position of the arctic front at this time. Figure 9b shows the various cloud layers that formed in response to the kinematic and thermodynamic features shown in Fig. 9a and the complicated interactions between these layers that were responsible for the precipitation. The presence of stratocumulus cloud above the arctic front (Fig. 9b) is consistent with the MM4 model trajectories that showed warm air moving northward and rising over the shallow arctic air (Fig. 8b). Note that the stratocumulus cloud tops rose to the north as the top of the arctic air rose. The stratocumulus bases also rose to the north as the cold, dry arctic air eroded the bases and evaporated the precipitation before it reached the ground. The underlying arctic air was also responsible for the rapid change of the surface precipitation from rain to snow. The aircraft encountered needles and sheathlike ice crystals in this stratocumulus cloud. The diffusional growth layer for these crystal types occurs at temperatures characteristic of those observed in the stratocumulus layer (Magono and Lee 1966). Thus, the crystals were generated in the stratocumulus layer associated with the arctic front.

The cumulus and cumulonimbus clouds observed from the aircraft were located below 500 mb and south of the boundary of cold-air advection aloft at 500 mb. The cumulus and cumulonimbus clouds had bases above 700 mb and produced dendrites and graupel. MM4 model trajectories show that the cold dry air that moved northward behind the boundary of cold-air advection aloft was lifted along the boundary of the warm-air advection above the arctic front. The resulting differential temperature advection led to destabilization of the midtroposphere in this region. When this air was lifted, the instability was released to form cumuliform clouds.

An altocumulus cloud layer was located north of the cold-air advection at 500 mb. Above this cloud layer was an altostratus layer. The aircraft flew between these two cloud layers where it encountered side planes, radiating assemblages of plates and sector ice crystals. These crystals grow at water saturation at temperatures colder than the diffusional growth layer of dendrites or needles. Therefore, these crystals must have been generated in the altostratus cloud.

The MM4 model trajectories showed that the air ahead of the boundary of cold-air advection aloft was

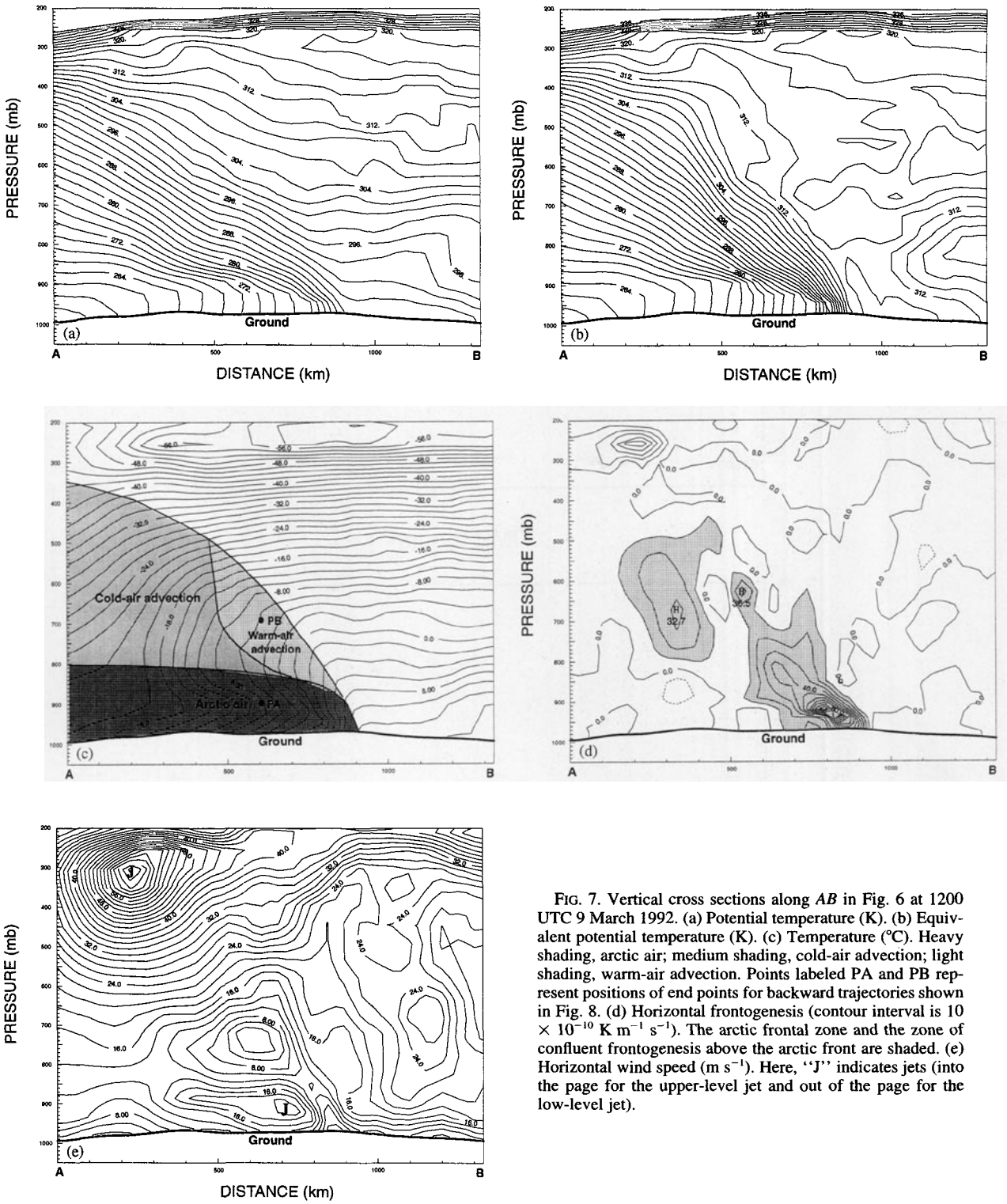

FIG. 7. Vertical cross sections along *AB* in Fig. 6 at 1200 UTC 9 March 1992. (a) Potential temperature (K). (b) Equivalent potential temperature (K). (c) Temperature (°C). Heavy shading, arctic air; medium shading, cold-air advection; light shading, warm-air advection. Points labeled PA and PB represent positions of end points for backward trajectories shown in Fig. 8. (d) Horizontal frontogenesis (contour interval is 10 $\times$ 10^{-10} K m^{-1} s^{-1}). The arctic frontal zone and the zone of confluent frontogenesis above the arctic front are shaded. (e) Horizontal wind speed (m s^{-1}). Here, "J" indicates jets (into the page for the upper-level jet and out of the page for the low-level jet).

rising as the boundary moved northward into the region of the cross section shown in Fig. 9. This lifting was produced by confluent frontogenesis in a deformation zone above 700 mb.

The stratocumulus cloud layer associated with the arctic air also produced precipitation on the ground in areas removed from the midlevel cumulonimbus. However, the ice crystals observed from the aircraft showed

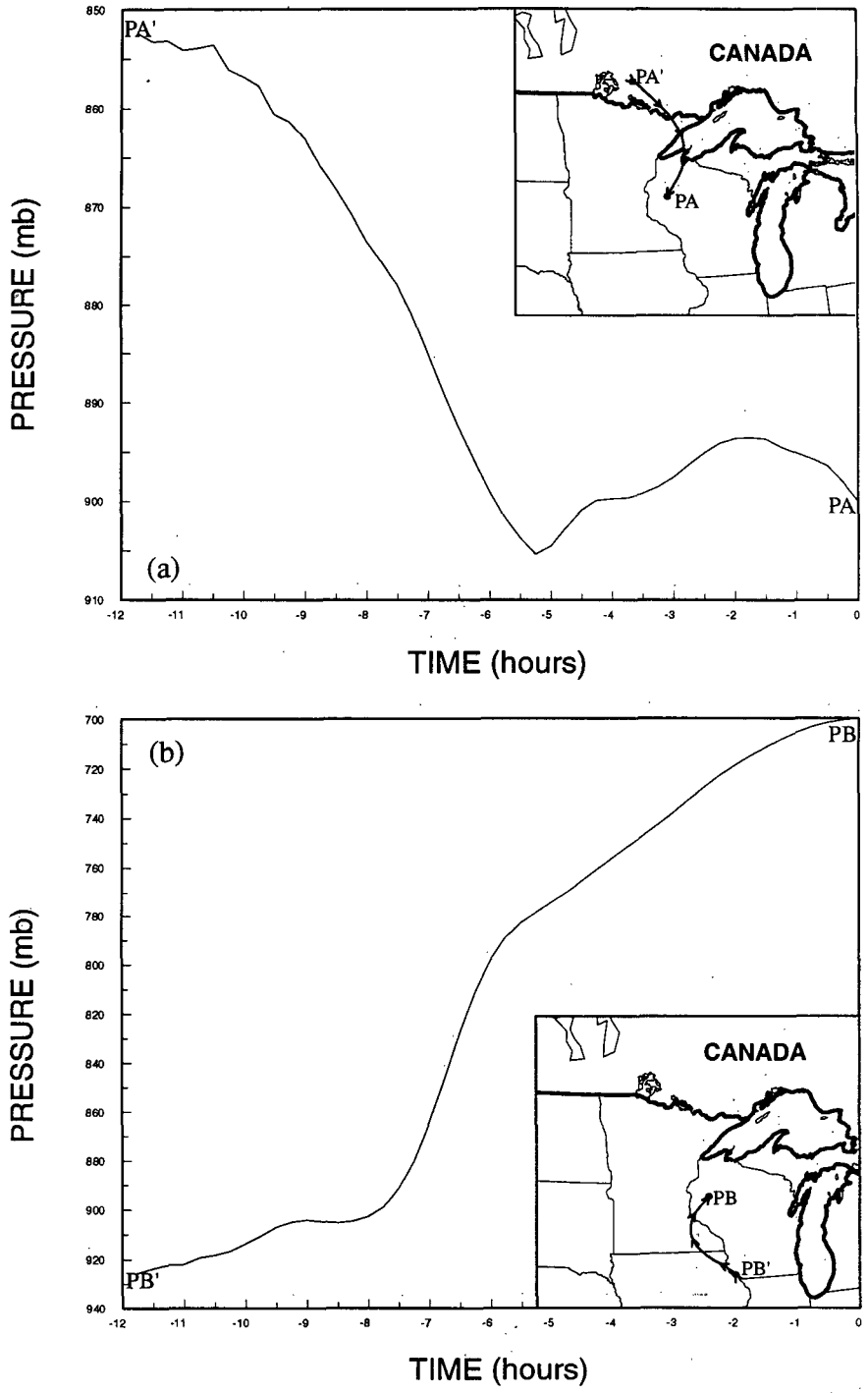

FIG. 8. (a) The 12-h backward air parcel trajectories in the vertical from PA′ to PA calculated from MM4 model simulation from 0000 UTC to 1200 UTC 9 March 1992. The endpoint PA is shown in Fig. 7c. The insert shows the horizontal trajectory of the parcel. (b) As for (a) but for PB′ to PB. The endpoint PB is shown in Fig. 7c.

that dendrites from the cumulonimbus were also present in the stratocumulus. In addition, crystals from the altostratus layer were falling through the flight level of the aircraft (~4.5 km) into the altocumulus cloud deck below and possibly into the stratocumulus. This "seeder–feeder" area was coincident with the

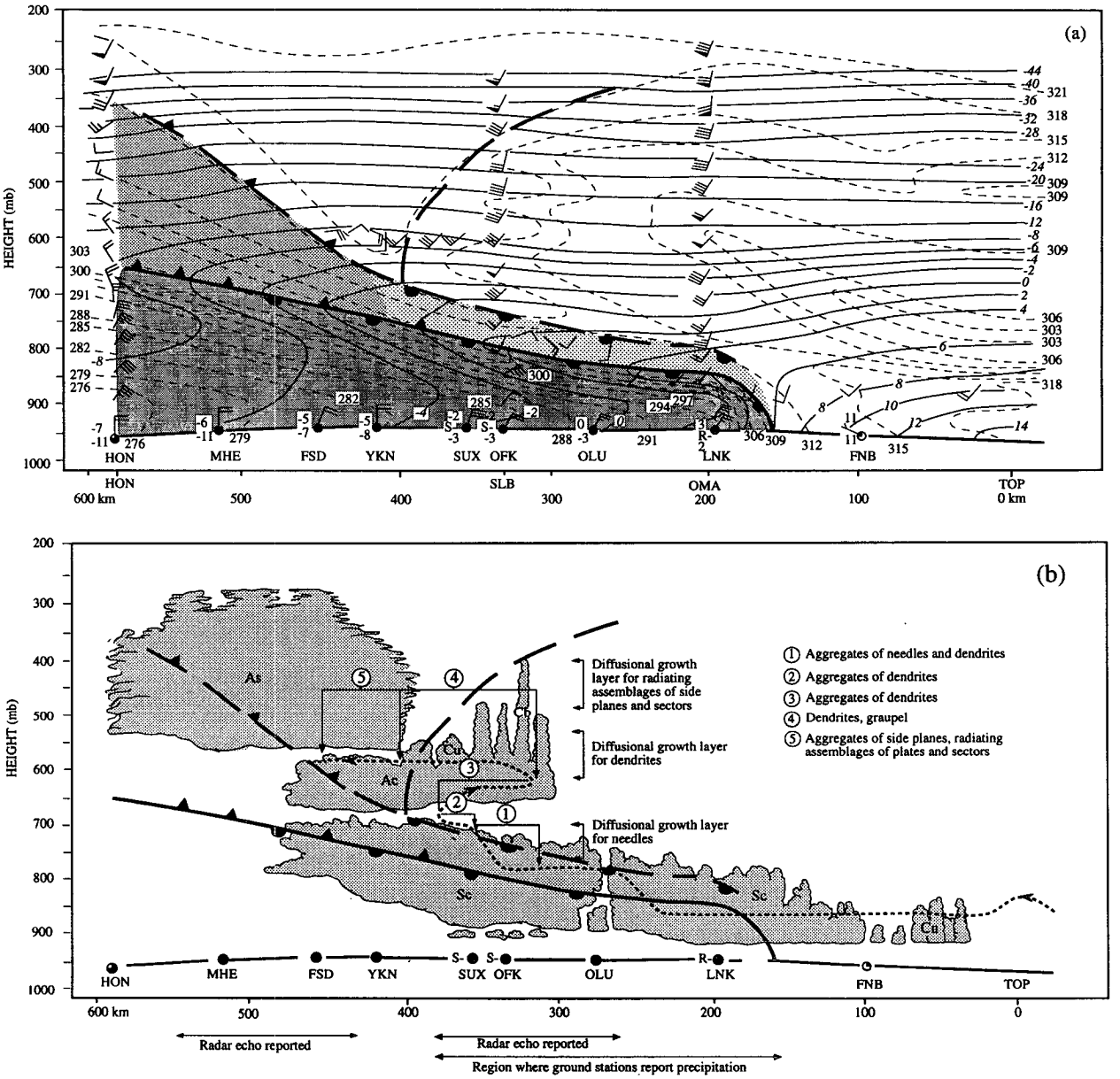

FIG. 9. Vertical cross sections from Topeka, Kansas (TOP), to Huron, South Dakota (HON), derived from measurements aboard the Convair C-131 aircraft. (a) Thermodynamic structure. Dashed lines are equivalent potential temperature (K) and continuous lines are temperature (°C). The heavy dashed line shows the leading edge of cold-air advection aloft and the heavy dashed line with frontal symbols shows the leading edge of the zone of confluent frontogenesis. The continuous heavy solid line with frontal symbols is the arctic front. Shadings as for Fig. 7c. (b) Schematic showing microphysical structure of the clouds associated with the arctic front, the zone of confluent frontogenesis, and cold-air advection aloft. The aircraft track is shown by the dotted line with arrows. Regions of radar echo and surface stations reporting precipitation are also shown. Shading shows clouds. Weather stations marked in the figure are HON (Huron, SD), MHE (Mitchell, SD), FSD (Sioux Falls, SD), YKN (Yankton, SD), SUX (Sioux City, IA), OFK (Norfolk, NE), OLU (Columbus, NE), LNK (Lincoln, NE), FNB (Fall City, NE), TOP (Topeka, KS), SLB (Storm Lake, IA), and OMA (Omaha, NE).

most widespread area of precipitation along the flight track.

A strong low-level jet, centered at about 920 mb and directed toward the southwest with a maximum wind of 21.4 m s^{-1}, was located behind and parallel to the arctic front (see Fig. 7e and station SLB in Fig. 9a). Since this jet was directed upslope over the elevated plains of western Nebraska, it enhanced the precipitation in Nebraska associated with the arctic front (see Fig. 5a). The low-level jet increased in intensity (see Fig. 11g) as the low-level pressure gradient force associated with the arctic front strengthened.

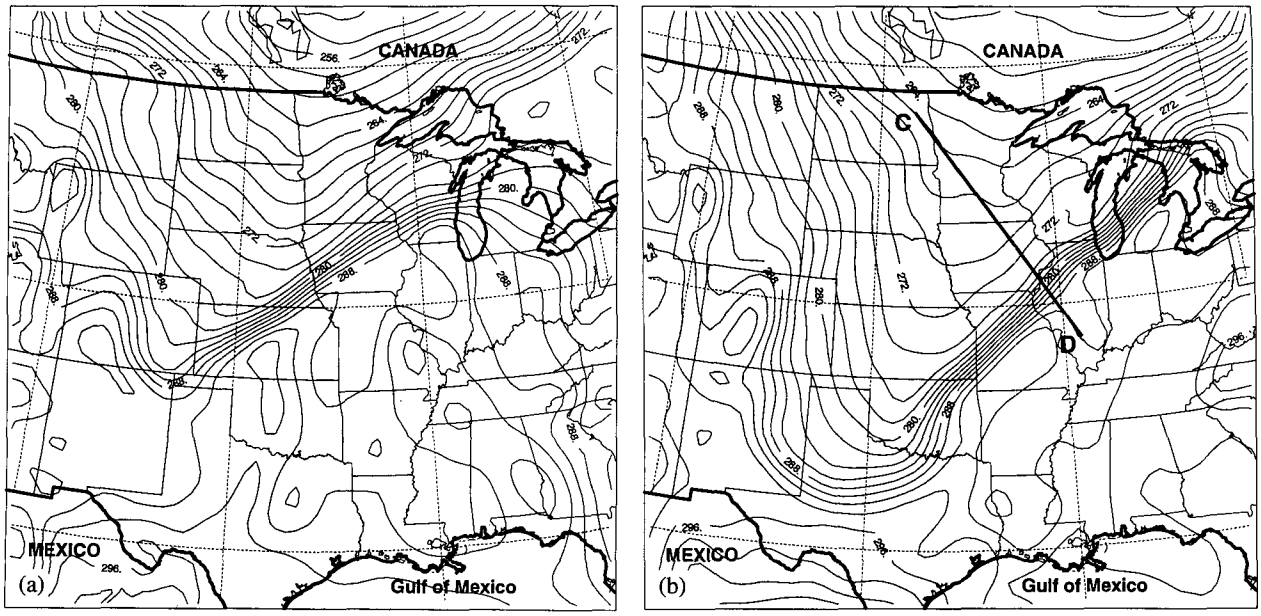

FIG. 10. MM4 model simulations of surface potential temperature (labeled in kelvins and contoured every 2 K) at (a) 1200 UTC 9 March and (b) 0000 UTC 10 March 1992.

b. 0000 UTC 10 March 1992

In the 12 h from 1200 UTC 9 March to 0000 UTC 10 March, significant changes took place in both the structure of the arctic front and the larger synoptic-scale environment in which it was embedded. These changes had a profound influence on the manner in which precipitation was generated and distributed at the arctic front.

Figures 10a and 10b show the MM4 12- and 24-h simulations of potential temperature at the surface. Clearly, a strong baroclinic zone existed at 1200 UTC 9 March (Fig. 10a). This zone expanded in length considerably over the next 12 h (Fig. 10b) as its southern edge surged southward along the Rockies and its northern portion moved gradually southeastward. As can be seen from a comparison of Figs. 10a and 10b, frontogenesis occurred along a considerable length of the arctic front. Most of the increase in the potential temperature gradient was due to a squeezing together of the 276- and 288-K isentropes, which approximately define the cold and warm sides of this surface frontal zone. Because of the differential advance of the northern and southern portions of this feature, a more subtle shift occurred in the direction of the potential temperature gradient from 329° at 1200 UTC 9 March to 316° at 0000 UTC 10 March. This slight change was part of a general backing of the potential temperature gradient vector over the history of this storm; this subsequently played an important role in the cyclogenesis that occurred along the east coast of the United States.

We will now examine some of the structural and dynamical characteristics of the arctic front at 0000 UTC 10 March using a representative vertical cross section through line *CD* in Fig. 10b. Figure 11a shows a vertical cross section of potential temperature θ along *CD*. The arctic front is extremely sharp and, once again, appears fairly deep in the θ field. The corresponding temperature cross section is shown in Fig. 11b. The inversion at the top of the arctic front (which is continuous and stronger than the weak inversion at the leading of the cold-air advection) is located at approximately 800 mb and is topped by significant baroclinity, as was the case at 1200 UTC 9 March. A significant difference between the baroclinic zone at this time and at 1200 UTC 9 March is that at 0000 UTC the baroclinic zone is characterized entirely by cold-air advection (e.g., see the 700-mb analysis shown in Fig. 12 and the 500-mb analysis shown in Fig. 2d). The short-wave trough to the north, which had previously resided in southern Canada, had by this time sagged southward into the northern plains states, eradicating the zone of warm-air advection that had existed over Wisconsin. In the absence of differential horizontal advection, the weaker confluence at 0000 UTC 10 March was not nearly as frontogenetical.

Figure 11c shows the equivalent potential temperature θ_e cross section along *CD*. By this time the high-θ_e air that had been advected from the southeast over the intervening 12 h was at the edge of the arctic front and pushing up over the surface position of the front. This high-θ_e wedge, coupled with a region of lower θ_e located between 650 and 500 mb, resulted in a layer of convective instability between 760 and 600 mb just behind the surface position of the arctic front. A MM4

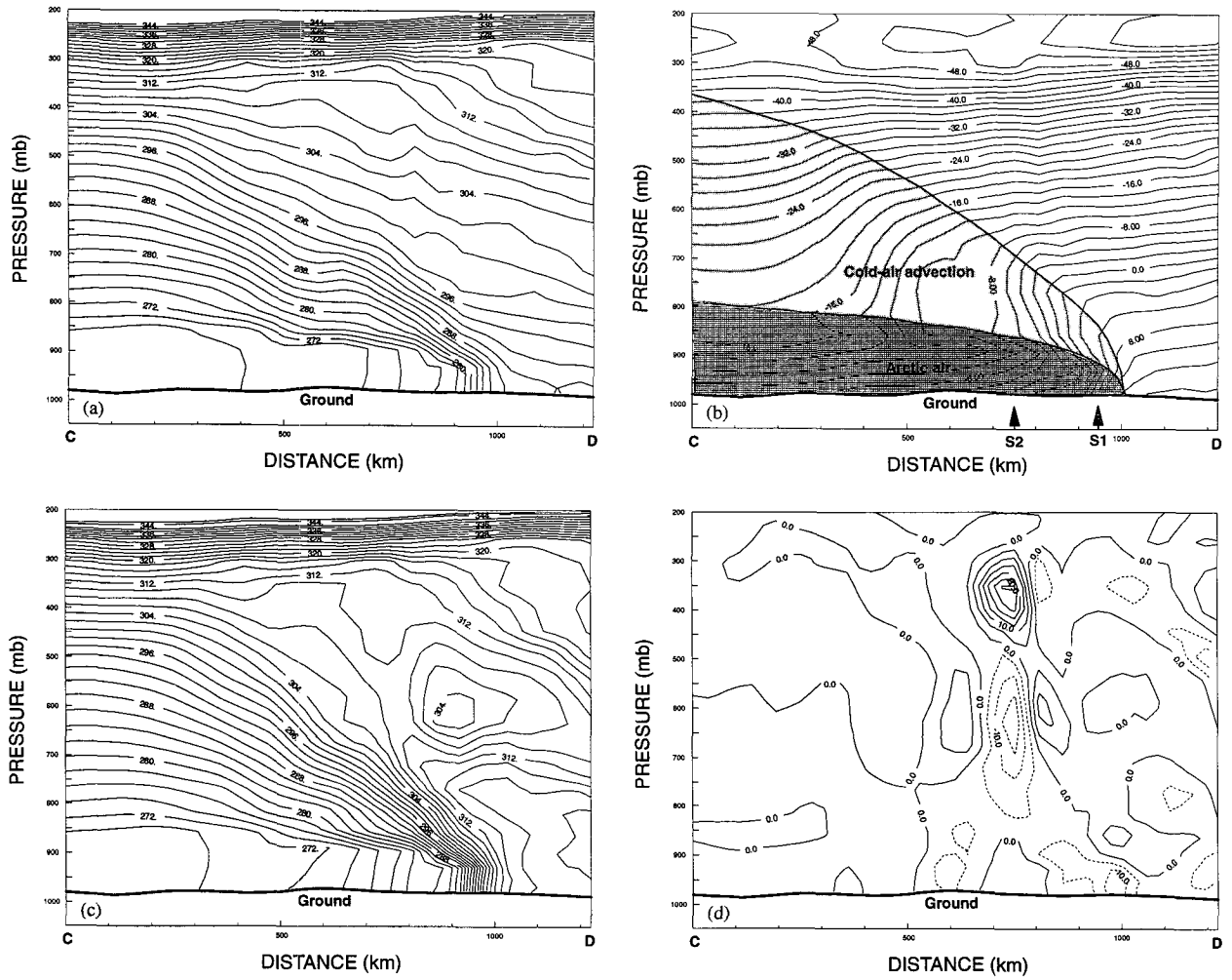

FIG. 11. Vertical cross section at 0000 UTC 10 March 1992 through line *CD* in Fig. 10b. (a) Potential temperature (K). (b) Temperature (°C). Shadings are same as in Fig. 7c. Soundings at S1 and S2 are shown in Fig. 13. (c) Equivalent potential temperature (K). (d) Divergence (contour interval is 5×10^{-5} s^{-1}; dashed lines indicate convergence and continuous lines divergence). (e) Vertical air velocity ($\omega = dp/dt$; contour interval is 1.0×10^{-3} mb s^{-1}); dashed lines indicate upward and continuous lines downward motion. Dark shading shows vertical velocity maxima associated with the arctic front, light shading shows vertical velocity maxima produced by the intrusion of short-wave trough at 500-mb into the region from the northwest. (f) Absolute vorticity (contour interval is 5×10^{-5} s^{-1}). (g) Horizontal wind speed (m s^{-1}). Here "J" indicates jets (into the page for the upper-level jet and out of the page for the low-level jet). (h) Contribution to frontogenesis from horizontal flow (contour interval is 10×10^{-10} K m^{-1} s^{-1}).

model sounding (S1 in Fig. 13) taken just north of the surface position of the arctic front (S1 in Fig. 11b) demonstrates the importance of this convective instability for precipitation formation. In this sounding, the layer from 800 to 750 mb was neutral for saturated air and unstable from 750 to 700 mb. The saturated air at 800 mb needed to be lifted only to 750 mb to reach its level of free convection. This lifting was easily provided by convergence along the arctic front, as shown in Fig. 11d. The vertical velocity field at this time has three distinct maxima, two of which (heavy shading in Fig. 11e) were associated with the arctic front. The third maxima (light shading in Fig. 11e), which was located north of the front near 500 mb, was produced by the intrusion of a sharp, short-wave trough into the region from the northwest. The model sounding (S2 in Fig. 13) taken at the location marked S2 in Fig. 11b shows that the air was stable below 700 mb and was neutral for moist air above this layer. The combination of mid- and upper-level neutrality, coupled with the dynamics of the encroaching upper trough, concentrated the upward movement of air and played a role in producing precipitation at and behind the arctic front.

Figure 11f shows the cross section of absolute vorticity along *CD*. The arctic front had vorticity values three to four times greater than the Coriolis parameter. A deep column of fairly strong vorticity was

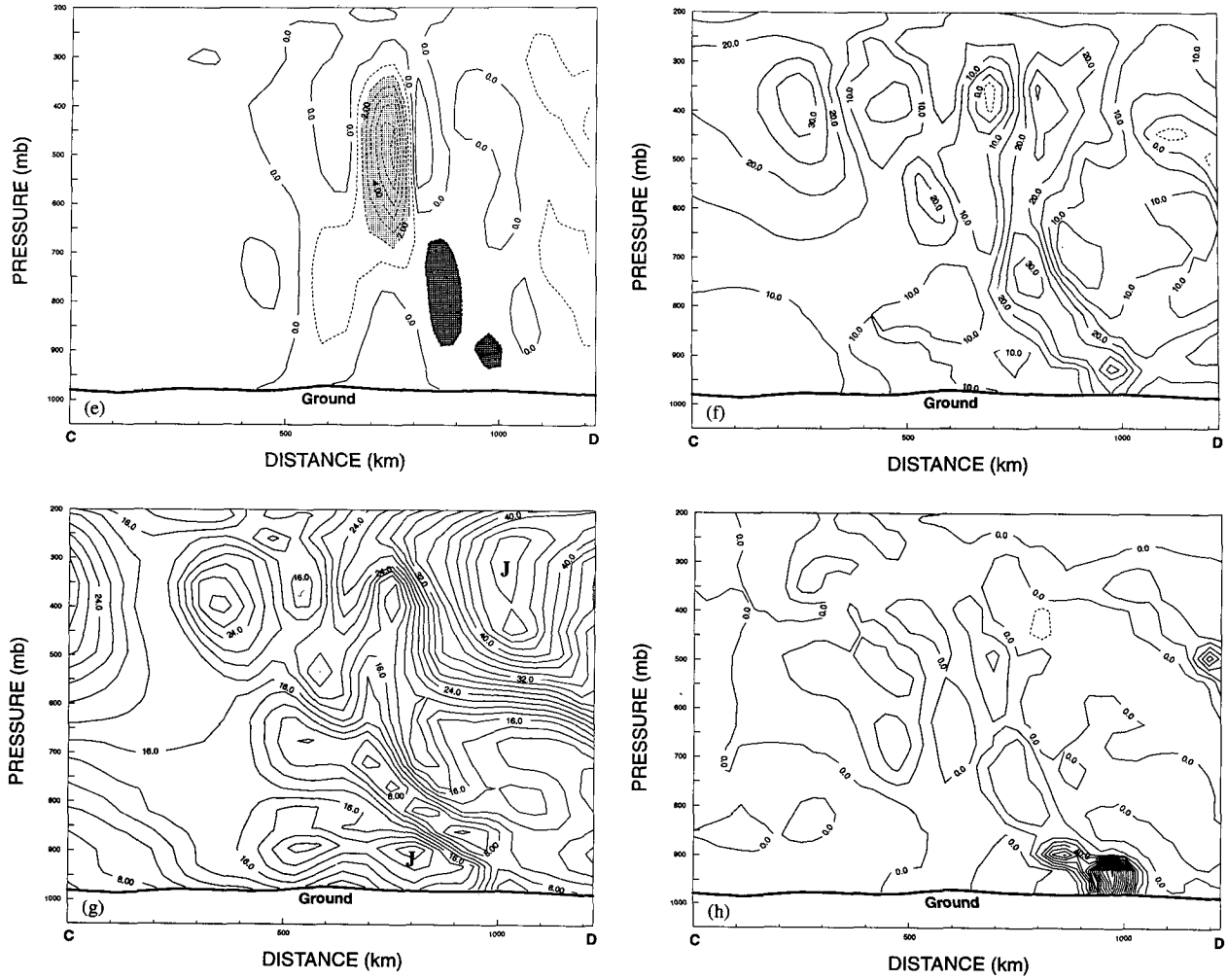

FIG. 11. (*Continued*)

associated with the wind speed maxima, and this culminated in a jet streak (Fig. 11g) that was exiting the plane of the cross section shown in Fig. 11f at this time.

As mentioned previously, up to this time significant frontogenesis had occurred along the arctic front. Figure 11h shows the contribution of the horizontal flow along *CD* to frontogenesis as simulated by the MM4 model. The most concentrated frontogenetical activity is in the lowest 100 mb and along the intersection of the frontal zone with the surface.

The NCDC accumulated precipitation from 2300 UTC 9 March to 0200 UTC 10 March (Fig. 5b) shows that the precipitation associated with the arctic front stretched from east of Kansas City to Lake Huron. This precipitation band was probably forced by the strong surface convergence associated with the frontogenesis of the arctic front enhanced (near Chicago) by the circulation associated with the entrance region of a jet streak aloft. The low cloud top indicated by the radar data suggests that the steady, light precipitation was largely accounted for by the arctic front itself, while localized regions of higher and more convective clouds were produced by the lifting of the mid-level, convectively unstable air by the upper-level disturbance.

4. Summary and conclusions

We have described in some detail the structure and evolution of an arctic front that affected the central United States from 0000 UTC 9 March to 0000 UTC 10 March 1992. This front swept rapidly southeastward through the central states, evolving as it went and acting, in concert with other processes, to spread precipitation across a large region.

The major results from this study can be summarized as follows.

- The arctic front, while extremely intense at the surface, was quite shallow and was capped by a strong

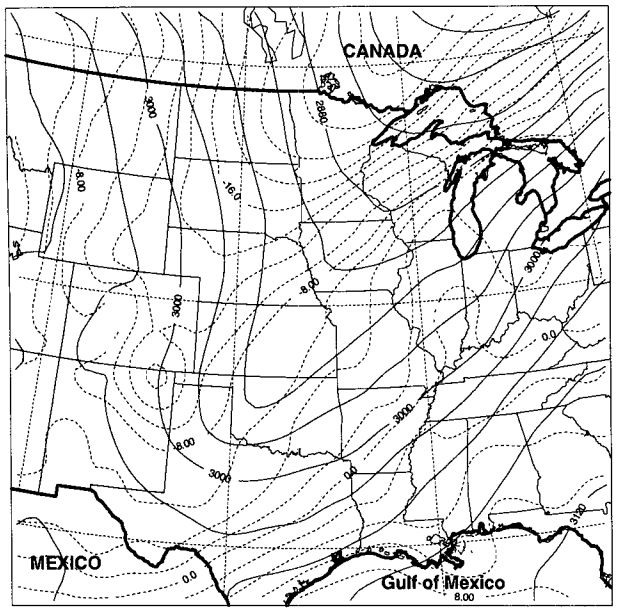

FIG. 12. As for Fig. 6 but for 0000 UTC 10 March 1992.

temperature inversion. As the front progressed southeastward, significant upslope motion in the foothills of the Rockies augmented larger-scale synoptic lifting to produce heavy snow in eastern Colorado.

- A deep region of cold-air advection, associated with a Canadian short-wave trough at 500 mb, was situated above the arctic frontal zone and extended from the low pressure center eastward. South of this zone was a southerly flow, which produced warm-air advection in the midtroposphere; this region of confluence was frontogenetical. The frontogenetical zone played an important role in augmenting precipitation associated with the arctic front. During the period of cold-air advection aloft, the arctic front was characterized by cold-air advection well north of its surface position and warm-air advection near its surface position.
- Passage of the arctic front west of the low pressure center and west of the drytrough was characterized by a sharp increase in wind speed and sharp decreases in temperature and dewpoint. The leading edge of the arctic front was located where the spacing of the isobars appreciably widened. These characteristics of arctic fronts, coupled with their proximity to drytroughs, often lead to a misanalysis of the drytrough as a cold front. To avoid this mistake, we recommend that arctic fronts be analyzed and tracked as separate features.
- A strong low-level jet was located behind and parallel to the arctic front. This jet was a manifestation of the steadily increasing pressure gradient that accompanied the intensifying arctic front. Since the jet was directed upslope over the high terrain of Nebraska, it enhanced precipitation in Nebraska that was associated with the arctic front.
- Cloud microphysical data showed that precipitation associated with the arctic front was augmented by ice crystals, from altocumulus and altostratus clouds aloft, falling into a lower stratocumulus deck. The upper cloud decks were associated with a midlevel, confluent frontogenetical zone and the large-scale, short-wave baroclinic disturbance that was overrunning the shallow arctic front. The location of the arctic front determined the transition from liquid to solid precipitation.
- The influence of arctic fronts on the meteorology of the United States is not restricted to their effects in the central states. Arctic frontal zones, such as the one described here, are preferred regions for cyclogenesis and can act as loci for the development of winter storms that move across the east coast of the United States. In a future paper in this series, we will examine the role of the arctic front described here in the development of a major winter storm in the eastern United States.

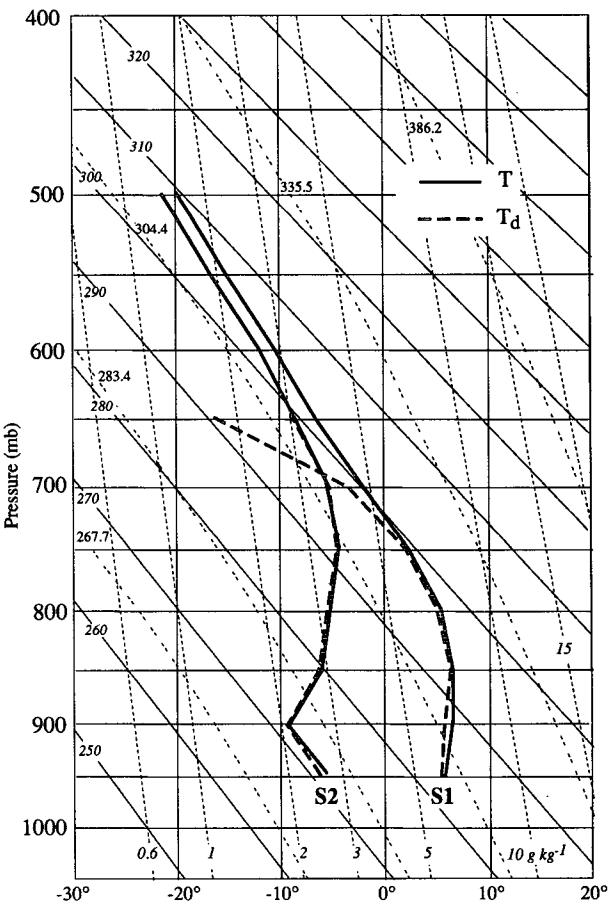

FIG. 13. MM4 model simulations of soundings at 0000 UTC 10 March for positions S1 and S2 shown in Fig. 11b. Temperature and dewpoint are plotted on a pseudoadiabatic diagram. Vertical solid lines are isotherms in degrees Celsius. Sloping solid lines are isentropes labeled in kelvins. Single-dashed lines are constant saturation mixing ratio in grams per kilogram. Double-dashed lines are pseudoadiabats, labeled in equivalent potential temperature in kelvins.

Acknowledgments. We thank all participants and sponsors of STORM-FEST. This research was supported by Grant ATM-9106235 from the Atmospheric Research Division of the National Science Foundation.

REFERENCES

Anthes, R. A., and T. T. Warner, 1978: Development of hydrodynamic models suitable for air pollution and other meso-meteorological studies. *Mon. Wea. Rev.*, **106,** 1045–1078.

——, E.-Y. Hsie, and Y.-H. Kuo, 1987: Description of the Penn State/NCAR Mesoscale Model Version (MM4). NCAR Tech. Note NCAR/TN-282+STR, 66 pp. [Available from the National Center for Atmosphere Research, P.O. Box 3000, Boulder, CO 80307-3000.]

Blackadar, A. K., 1979: *High Resolution Models of the Planetary Boundary Layer.* Advances in Environmental Science and Engineering, Vol. 1, No. 1, Gordon and Breach Science Publishers, 50–85.

Bluestein, H. B., 1993: Synoptic–Dynamic Meteorology in Midlatitudes. Volume 2, *Observations and Theory of Weather Systems.* Oxford University Press, 594 pp.

Hobbs, P. V., J. D. Locatelli, and J. E. Martin, 1990: Cold fronts aloft and the forecasting of precipitation and severe weather east of the Rocky Mountains. *Wea. Forecasting,* **5,** 614–626.

Locatelli, J. D., J. E. Martin, and P. V. Hobbs, 1995: Structure and evolution of winter cyclones in the central United States and their effects on the distribution of precipitation. Part III: A rainband associated with cold frontogenesis aloft. *Mon. Wea. Rev.,* in press.

Magono, C., and C. W. Lee, 1966: Meteorological classification of natural snow crystals. *J. Fac. Sci. Hokkaido Univ. Ser. 7,* **2.**

Martin, J. E., J. D. Locatelli, P. V. Hobbs, P.-Y. Wang, and J. A. Castle, 1995: Structure and evolution of winter cyclones in the central United States and their effects on the distribution of precipitation. Part I: A synoptic-scale rainband associated with a dryline and lee trough. *Mon. Wea. Rev.,* **123,** 241–264.

Ogura, Y., and D. Portis, 1982: Structure of the cold front observed in SESAME-AVE III and its comparison with the Hoskins–Bretherton frontogenesis model. *J. Atmos. Sci.,* **39,** 2773–2792.

Rossby, C.-G., and R. H. Weightman, 1926: Application of the polar-front theory to a series of American weather maps. *Mon. Wea. Rev.,* **54,** 485–496.

Showalter, A. K., 1939: Further studies of American air-mass properties. *Mon. Wea. Rev.,* **67,** 204–218.

Wexler, H., 1936: Cooling in the lower atmosphere and the structure of polar continental air. *Mon. Wea. Rev.,* **64,** 122–136.

Zhang, D.-L., and R. A. Anthes, 1982: A high-resolution model of the planetary boundary layer—Sensitivity tests and comparison with SESAME-79 data. *J. Appl. Meteor.,* **21,** 1594–1609.